Biomaterials 125 (2017) 13–22

Contents lists available at ScienceDirect

Biomaterials

journal homepage: www.elsevier.com/locate/biomaterials

Crossing kingdoms: Using decellularized plants as perfusable tissue engineering scaffolds

Joshua R. Gershlak [a], Sarah Hernandez [b], Gianluca Fontana [c], Luke R. Perreault [a], Katrina J. Hansen [a], Sara A. Larson [b], Bernard Y.K. Binder [d], David M. Dolivo [b], Tianhong Yang [e, f], Tanja Dominko [b, g], Marsha W. Rolle [a], Pamela J. Weathers [b], Fabricio Medina-Bolivar [e, f], Carole L. Cramer [e, f], William L. Murphy [c, h, i], Glenn R. Gaudette [a, *]

[a] Biomedical Engineering, Worcester Polytechnic Institute, Worcester, MA, United States
[b] Biology and Biotechnology, Worcester Polytechnic Institute, Worcester, MA, United States
[c] Orthopedics and Rehabilitation, University of Wisconsin School of Medicine and Public Health, Madison, WI, United States
[d] Department of Surgery, University of Wisconsin School of Medicine and Public Health, Madison, WI, United States
[e] Department of Biological Sciences, Arkansas State University, Jonesboro, AR, United States
[f] Arkansas Biosciences Institute, Arkansas State University, Jonesboro, AR, United States
[g] Center for Biomedical Sciences and Engineering, University of Nova Gorica, Slovenia
[h] Biomedical Engineering, University of Wisconsin-Madison, Madison, WI, United States
[i] Material Sciences and Engineering, University of Wisconsin-Madison, Madison, WI, United States

ARTICLE INFO

Article history:
Received 4 October 2016
Received in revised form
8 February 2017
Accepted 9 February 2017
Available online 10 February 2017

Keywords:
Regenerative medicine
Tissue engineering
Decellularization
Perfusable scaffold
Plants

ABSTRACT

Despite significant advances in the fabrication of bioengineered scaffolds for tissue engineering, delivery of nutrients in complex engineered human tissues remains a challenge. By taking advantage of the similarities in the vascular structure of plant and animal tissues, we developed decellularized plant tissue as a prevascularized scaffold for tissue engineering applications. Perfusion-based decellularization was modified for different plant species, providing different geometries of scaffolding. After decellularization, plant scaffolds remained patent and able to transport microparticles. Plant scaffolds were recellularized with human endothelial cells that colonized the inner surfaces of plant vasculature. Human mesenchymal stem cells and human pluripotent stem cell derived cardiomyocytes adhered to the outer surfaces of plant scaffolds. Cardiomyocytes demonstrated contractile function and calcium handling capabilities over the course of 21 days. These data demonstrate the potential of decellularized plants as scaffolds for tissue engineering, which could ultimately provide a cost-efficient, "green" technology for regenerating large volume vascularized tissue mass.

© 2017 The Authors. Published by Elsevier Ltd. This is an open access article under the CC BY-NC-ND license (http://creativecommons.org/licenses/by-nc-nd/4.0/).

1. Introduction

The need for organs and tissues available for transplantation far exceeds their availability. More than 100,000 patients can be found on the donor waiting list at any given time and an average of 22 people die each day while waiting for a donor organ or tissue to become available [1]. Tissue engineering has made significant strides over the past decade through the development of tissue grafts, increasing the potential number of viable solutions for these patients. However, there are still issues impeding their translation into the clinic. One of the major factors currently limiting clinical applicability of tissue engineered solutions is the lack of a functional vascular network [2]. Without a viable vascular network, the 100–200 μm oxygen diffusion limit within tissues cannot be overcome, consequently restricting the size of graft that can be engineered and retain viability. Most current bioengineering techniques are unable to create patent perfusion vessels. Techniques such as the loading of scaffolds with pro-angiogenic factors [3], cellular-guided vascular network formation [4], and microfabricated designs [5] have demonstrated limited success in fully recapitulating native vasculature. Furthermore, microvasculature

* Corresponding author.
E-mail address: gaudette@wpi.edu (G.R. Gaudette).

http://dx.doi.org/10.1016/j.biomaterials.2017.02.011
0142-9612/© 2017 The Authors. Published by Elsevier Ltd. This is an open access article under the CC BY-NC-ND license (http://creativecommons.org/licenses/by-nc-nd/4.0/).

(<10 μm in diameter) cannot be functionally fabricated with current biofabrication techniques, such as 3-D printing.

Instead of attempting to engineer a vascular network, current focus has shifted towards bio-inspired approaches, further driven by the advent of perfusion-based techniques for decellularization [6]. Decellularization removes cellular material from a tissue or organ leaving behind an acellular scaffold consisting of extracellular matrix (ECM), the composition of which depends on the tissue or organ from which it was derived [7], while preserving an intact vascular network [8]. By removing the cellular material of a donor's tissue, a decellularized graft would be rendered non-immunogenic while retaining gross organ structure [9]. Decellularized tissues and organs can then be recellularized with a patient's own cells to create an autologous graft [8]. Native biochemical composition and hierarchical tissue structure of a potential decellularized graft are derived from the donor of the tissue or organ. This inherently leads to inconsistency among tissues or organs derived from different patients, or decellularized using different methods, due to confounding variables such as age, organismal or tissue pathology, and the specifics of the decellularization protocol [7,10,11]. In particular, protein compositional analysis through mass spectrometry has shown drastic differences in the composition of decellularized tissues between different patients [12,13]. Decellularized mammalian tissues are also in short supply and, even when available, are expensive. Furthermore, a considerable amount of additional research needs to be conducted before entire decellularized organs can be considered as a practical option clinically [14]. Consequently, a more consistent, cost-effective and readily available tissue source for decellularization would yield improved prospects by increasing viable numbers of grafts at a significantly lower cost.

Most current bioengineering approaches are limited by the physical and intellectual isolation of basic research in different organisms to their respective biological kingdoms. This critical challenge can be overcome by exploiting *cross-kingdom* contributions within the same bioengineered platform. Plants and animals exploit fundamentally different approaches to transporting fluids, chemicals, and macromolecules, yet there are surprising similarities in their vascular network structures (Fig. 1). Plant vasculature follows Murray's Law [15], which is the physiological law describing the tapered, branching network design of the human cardiovascular system [16]. Structures within plant tissue [17], like human tissue [18], exhibit varied mechanical properties, enabling varied functions. Plant cell walls are composed of a variety of polysaccharides, the most prominent of which are cellulose, pectin, and hemicellulose [19]. Cellulose, which is the most abundant component of plant cell walls, is a well-studied biomaterial for a variety of clinical applications [20]. Cellulose is biocompatible and has been shown to promote wound healing [21]. Furthermore, cellulosic tissue engineering scaffolds derived from decellularized apple slices have shown the ability for mammalian cell attachment and proliferation [22] and were found to be biocompatible when implanted subcutaneously *in vivo* [23]. Pectin [24] and hemicellulose [25] have also been studied as biomaterials for bone tissue engineering and wound healing, respectively. The innate similarities and apparent biocompatibility of plant ECM spurred us to look *across kingdoms* and investigate whether plants and their innate vasculatures could serve as perfusable scaffolds for engineering human tissue. Decellularization techniques were applied to different plant species and tissues in order to generate acellular, pre-vascularized tissue engineering scaffolds. The abundance and rapid growth of many plant species also provides for a less costly, more plentiful and sustainable scaffold material.

2. Materials and methods

Plant Decellularization: Spinach and parsley were acquired from a local market. *Artemisia annua* leaves (SAM cultivar, specimen voucher MASS 00317314) were harvested from soil-grown plants. Peanut hairy roots were generated through *Agrobacterium rhizogenes*-mediated genetic transformation [26,27]. Decellularization for the different plant types was adapted from whole organ perfusion decellularization techniques [6–8]. Spinach leaves were cannulated through the petiole and parsley stems were cannulated via the basipetal end of the stem segment. Cuticles were removed from the plants via serial treatment with hexanes (98%, Mixed Isomers, Alfa Aesar, Haverhill, MA) and 1x PBS. A 10% sodium dodecyl sulfate (SDS) in deionized water solution was perfused through the cannulas for 5 days, after which they were perfused with a 0.1% Triton-X-100 in a 10% sodium chlorite bleach (Aqua-Tab, Beckart Environmental, Kenosha, WI) in deionized water solution for 48 h. Sterile deionized water was then perfused for an additional 48 h. Perfusion was accomplished from a constant pressure head of 152 mmHg and flow was initiated by gravity. *A. annua* and peanut hairy roots were decellularized using the same technique but instead of cannulation and perfusion, they were soaked in the solutions. After decellularization was complete, tissues were stored in sterile deionized water at 4 °C until needed for up to two weeks.

Histological Analysis: Leaf samples were cut into ~1 cm squares, preferentially cut with the main vascular channel of the leaf down the middle of the square. Roots and stems were cut into approximately ~1 cm length pieces. Tissue samples were fixed overnight in an ATP-1 automatic tissue processor (Triangle Biomedical Sciences, North Carolina) and then embedded in paraffin.

Paraffin blocks were sectioned at 14 μm. Samples that were stained using Sass's Safranin and Fast Green protocol for plant staining were done as previously reported [28]. In short, sections were stained for 1 h in aqueous 1% (w/v) Safranin-O, and then rinsed in deionized water for approximately 5 min, or until all residual dye was removed from the sections. Sections were dehydrated in 70%, then 95% ethanol and dipped for 10 s in Fast Green FCF (0.1% w/v in 95% ethanol). Sections were washed in two changes of 100% ethanol (2 min/step) and cleared in two changes of xylene (2 min/step). Samples were stained for lignin for 10 min in a saturated solution of phloroglucionol in 20% hydrochloride, as previously reported [29]. Samples were visualized through use of a DMLB2 upright microscope (Leica Microsystems, Buffalo Grove, IL).

Scanning Electron Microscope Imaging: The preparation of samples for Scanning Electron Microscopy (SEM) analysis consisted of fixation with 1.5% glutaraldehyde in freshly prepared 0.07 M sodium cacodylate buffer for 2 h. The samples were then rinsed in 0.07 M sodium cacodylate with the addition of 2.5% sucrose and dehydrated by immersion in a graduated series of ethanol in H_2O, serially in the following concentrations: 30, 50, 80, and 95%. Then samples were immersed in hexamethyldisilazane (HDMS) in ethanol serial solutions in the following concentrations: 30, 50, 80, and 95%. The samples were left to dry on the sample holder and then gold sputter coated prior to imaging in SEM.

DNA/Protein Quantification: Both native and decellularized leaves were put in centrifuge tubes in a liquid nitrogen bath and ground with a pestle. Fragments were further processed by pulling through a 25-gauge syringe needle and by sonication with 5 pulses performed 3 times to reduce leaf fragment size. DNA was then measured using a CyQUANT Direct Cell Proliferation Assay (Thermo Fisher, Waltham, MA) and protein was measured using a Coomassie (Bradford) Protein Assay Kit (Thermo Fisher). Concentrations were determined using a Victor3 spectrophotometer (Perkin Elmer, Waltham, MA).

Perfusion Studies: Decellularized spinach leaves were removed

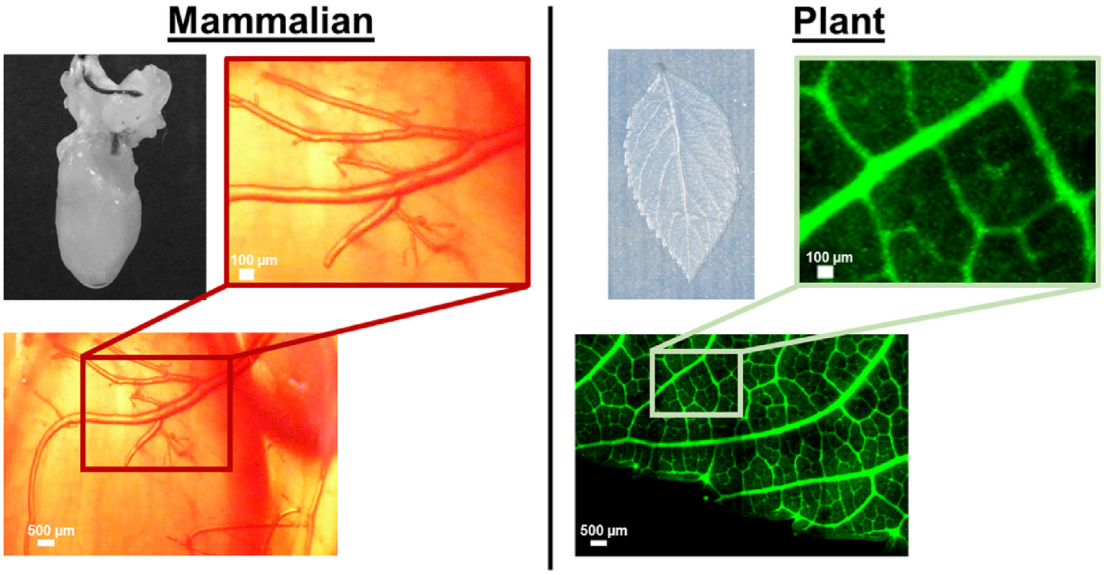

Fig. 1. Comparison of animal and plant vascular network pattern branching and structures. A rat heart was decellularized, as previously described [6], and was perfused with a Ponceau Red stain to visualize the vasculature. A *Buddleja davidii* leaf was perfused with fluorescein-labeled PEGDA to visualize the leaf vasculature.

from refrigerated storage and were dried with Kimwipes prior to the start of the different perfusion studies. A 0.1% Ponceau Red (Sigma Aldrich, Saint Louis, MO) in 1% acetic acid solution was perfused through the cannula attached to the petiole of each decellularized spinach leaf. Ponceau red was perfused from a constant pressure of 152 mmHg via gravity driven flow. Images were taken before and after cannulation to investigate the remaining patency of the decellularized leaf vasculature.

Microspheres (1, 10, 50, and 100 μm sized) (Phosphorex Inc., Hopkinton, MA) were used to determine the inner diameter flow limitations of the leaf vasculature. Perfusion was accomplished through a syringe-pump with a flow rate of 200 μl/min. Prior to the microsphere perfusion, blank fluid was perfused through the leaf in order to measure any autofluorescence from the perfusate. A serial perfusion of different singular fluorescent microsphere sizes was conducted beginning with smallest to largest diameters. After perfusion was completed, the runoff of each individually sized microsphere was collected and analyzed using a Victor3 microplate reader (Perkin Elmer) against a known standard curve for each individually sized microsphere. There was some fluid loss experienced when collecting the runoffs from the perfusion. This fluid loss can be attributed to the porous structures of the leaves causing small volumes of liquid to collect in the leaf. For the high-speed videos, a HiSpec4 high-speed camera (FastTec, San Diego, CA) was attached to a DMIL inverted microscope (Leica Microsystems, Buffalo Grove, IL) and high-speed videos were taken at 60 frames per second. A mixture of the different microspheres was perfused for the videos. Microspheres flowing through the vasculature were false colored white to heighten the contrast between sphere and background. Confocal images of leaves verified microsphere entrapment. Images were acquired using a SP5 Point Scanning Confocal (Leica Microsystems).

***Mechanical Testing*:** Native and decellularized spinach leaves were cut into a 1 × 2 cm dogbone shape. Leaves were loaded into the grips of the mechanical tester with the apical end of the leaf being upright. An ElectroPulse E1000 tester (Instron Corp., Norwood, MA) was used to uniaxially stretch the leaves. Leaves were stretched at a constant strain of 10 mm/mm until failure. Maximum tangent modulus, ultimate tensile strength, and strain at failure were calculated. Maximum tangent modulus was established by fitting a line to the maximal sloped linear region of the stress-strain graph. Ultimate tensile strength and strain at failure were calculated from the generated stress-strain graphs.

***Mammalian Cell Culture and Seeding*:** For only HUVEC and hPS-CM attachment experiments, leaf scaffold stems were coated with fibronectin. Fibronectin (from bovine plasma, Sigma Aldrich) was injected through the cannula of the leaf scaffolds at a concentration of 10 μg/mL and allowed to coat for 24 h in a standard incubator. Prior to HUVEC seeding, leaves were injected with sterile PBS to wash away any non-coated fibronectin from the leaf. For hPS-CM seeding, fibronectin was applied to the surface of the leaf at the same concentration and incubation time. Prior to hPS-CM seeding, leaves were washed in sterile PBS.

HUVECs (CRL-1730, American Type Culture Collection (ATCC), Manassas, Virginia) were maintained using an Endothelial Cell Growth Kit −VEGF (ATCC) according to the manufacturer's instructions. HUVECs were fluorescently labeled through uptake of acetylated low-density lipoprotein (Dil-Ac-LDL) (Thermo Fisher). Labeling occurred by incubating HUVECs for 4 h at 37 °C in medium containing 10 μl/mL Dil-Ac-LDL. A 500 μl aliquot containing 375,000 labeled HUVECs was injected into the cannulated stem of a decellularized spinach leaf. HUVECs were allowed 24 h for adherence and were then subsequently washed with PBS. Adherent HUVECs were visualized using a Rhodamine filter on an SP5 Point Scanning Confocal (Leica Microsystems).

Viability of HUVECs after recellularization was determined using a LDL uptake assay. Unlabeled HUVECs were injected into the cannulated stem as previously described; 24 h after seeding, HUVEC seeded stems and unseeded stems were moved into medium containing 10 μl/mL Dil-Ac-LDL for 4 h at 37 °C. Images of stems were acquired prior to LDL incubation, 24 h after the end of incubation, and 48 h after the end of incubation using a Rhodamine filter on a DMIL inverted microscope (Leica Microsystems).

P4–P8 hMSCs (Lonza, Walkersville, Maryland) were maintained in MSCGM growth medium (Lonza) until they reached 70–80% confluence. The hMSCs were treated for 24 h with MSCGM medium supplemented with 8.2 nM QDot 655 ITK carboxyl Quantum Dots (Thermo Fisher). After the 24 h treatment, the quantum dot-loaded hMSCs were gently washed with PBS and maintained in growth medium until use. Loaded hMSCs were seeded on the surface of the

decellularized spinach leaves for 24 h to allow for attachment. Adherent hMSCs were visualized using QDot 655 filter settings on the SP5 Point Scanning Confocal.

Embryonic stem cell derived cardiomyocytes (hPS-CMs) (provided by Dr. Michael LaFlamme, University of Toronto, Toronto, Ontario) [30] were maintained in RPMI medium containing 2% B27, 1% Pen/Strep, and 1% L-Glutamine (Thermo Fisher). The hPS-CMs were thawed and immediately seeded onto the surface of spinach leaves. Cells were given 24 h of seeding before medium was replaced, and were subsequently replaced every 48 h for the duration of 21 days.

***hPS-CM Contraction and Fluorescent Analysis*:** A HiSpec4 high speed camera (FastTec, San Diego, CA) was attached to a DMIL inverted microscope (Leica Microsystems, Buffalo Grove, IL) and videos of contracting hPS-CM clusters were taken at 60 frames per second. A speckle-based tracking algorithm, high density mapping [31], was applied to the contraction videos. The algorithm measures subpixel level displacement of a random light intensity object. From these subpixel displacements, the contractile strain can be calculated over a region of interest. Fluorescent videos were recorded at 71 frames per second and were analyzed through a custom MATLAB code, which measures the relative change in intensity over time.

***Statistical Analysis*:** All results are presented as mean ± standard deviation. Statistical comparisons were made through either the use of a Student's t-test or a one-way ANOVA with a Tukey's post-hoc test. Both statistical tests were performed within SigmaPlot (Systat Software Inc., San Jose, CA). Statistical significance was determined to be $p < 0.05$.

3. Results

3.1. Preparation and characterization of decellularized plant scaffolds

The natural structure of higher plants allows for the transport of nutrients via xylem and phloem to distal cells, e.g. from roots to leaves and leaves to roots or other leaves. To explore the potential for a plant-based tissue engineered scaffold, perfusion decellularization [6] was adapted for use with *Spinacia oleracea* (spinach) leaves. Spinach leaves were used as a model species due to their ready availability, their vascular network pattern and density, and their wide diameter petiole. Spinach leaf petioles were cannulated (Fig. S1) and then perfused with decellularization solution (10% sodium dodecyl sulfate (SDS) in deionized water) for 5 days, followed by 2 days of perfusion with clearing solution (0.1% TritonX-100, 10% sodium chlorite in deionized water). One day after initiation of the decellularization process, the leaves began to lose their green color due to the loss of chlorophyll, denoting loss of chloroplasts from the leaf tissue (Fig. 2A and B). Leaves became translucent with a green hue by Day 5 (Fig. 2C). The addition of sodium chlorite sterilized the tissue while also removing any residual chlorophyll, resulting in a colorless and translucent leaf by Day 7 (Fig. 2D). Histological analysis identified cells with nuclei and chloroplasts in native leaves (Fig. 3, A and C), neither of which was seen in their decellularized counterparts (Fig. 3, B and D). Furthermore, lignin, which is a major biopolymeric component of the leaf vasculature, was present before and after decellularization as shown by additional histological staining (Fig. S10). Decellularized spinach leaves maintained the same pattern and density of vascular networks seen in native leaves (Fig. 3E and F) when imaged by scanning electron microscopy (SEM), indicating that the decellularization process did not affect the topographical properties of the surface of the leaf. Neither decellularization nor clearing solution alone was able to completely decellularize the leaves (Fig. S2), indicating that both anionic and non-ionic detergents may be needed for complete removal of plant cellular material.

Decellularized leaves contained significantly less DNA (9.4 ± 1.3 vs. 1129 ± 217.3 ng DNA/mg tissue, Fig. 3G) and significantly less protein when compared to native leaves (2.4 ± 0.6 vs. 19.1 ± 1.9 μg protein/mg, Fig. 3H). These data demonstrated that the plant decellularization process removed nearly all of the DNA and protein. The levels of remaining DNA satisfy a minimal requirement determined to classify a tissue as decellularized (<50 ng DNA per mg tissue) [32]. The kinetics of protein removal demonstrated a rapid and significant decrease of protein content during the first 10 min. The protein levels decreased further during the subsequent days and reached the lowest concentration after 3 days of decellularization (Fig. S3). After 5 days of perfusion, the standard deviation between protein levels in different samples was found to be negligible and thus 5 days of perfusion with the decellularization solution was chosen as the standard time.

For robust characterization of a tissue scaffold, it is imperative to examine the mechanical properties of the scaffold material, as these properties govern the ability of the tissue to function. When compared to native leaves, decellularized leaves displayed significantly lower ultimate tensile strength ($p = 0.00925$) and strain at failure ($p = 0.000287$) during uniaxial tensile mechanical analysis (Fig. S4). Despite the apparent loss of mechanical integrity, maximum tangent modulus for decellularized spinach leaves (0.3 MPa) was within the range of normal decellularized human cardiac tissue (0.2–0.5 MPa) [8].

We also explored the applicability of this technique to other plant species and tissues. *Petroselinum crispum* (parsley) stems, *Arachis hypogaea* (peanut) hairy roots, and *Artemisia annua* leaves were also successfully decellularized (Fig. 3I) thereby suggesting widespread potential for using a variety of plant species and tissues for decellularization. Histological examination of these different plant systems was also conducted and yielded similar results as those seen in spinach leaves (Fig. S5), where there is a noted loss of nuclear material while maintaining gross plant microarchitecture. Hairy roots and *Aretemisia annua* were soaked in the decellularization and clearing solutions as opposed to perfusion due to their delicate vasculature. DNA levels of *A. annua* were also measured in order to verify that soaking performed the same levels of decellularization as perfusion (Fig. S5).

3.2. Assessment of leaf vasculature patency post-decellularization

A major advantage of using the decellularized leaf as a scaffold for tissue engineering is the innate vasculature. We thus sought to determine whether the leaf vasculature remained intact and patent after the decellularization process. Ponceau Red was perfused through the cannula of decellularized spinach leaves. The Ponceau Red perfused throughout the entirety of the leaf vasculature, with some minor leakage observed (Fig. 4A; Movie S1). The perfusate also flowed into and through the smaller branches of the leaf vein (Fig. 4B) indicating that the microvasculature of the leaf remained fairly intact.

Supplementary video related to this article can be found at http://dx.doi.org/10.1016/j.biomaterials.2017.02.011

For a vascularized tissue engineered scaffold to be clinically relevant, the inner diameter of any mimetic vessels must allow for blood flow. Human capillaries have vessel diameters between 5 and 10 μm [33] that support the flow of the 6–8 μm diameter red blood cells [34]. To predict whether the vascular network of a decellularized leaf would support flow of such cells, leaf vasculature was perfused with medium containing fluorescent microspheres of various sized diameters. This method allows for evaluation of both the diameter and patency of any given vessel. Videos (Movie S2)

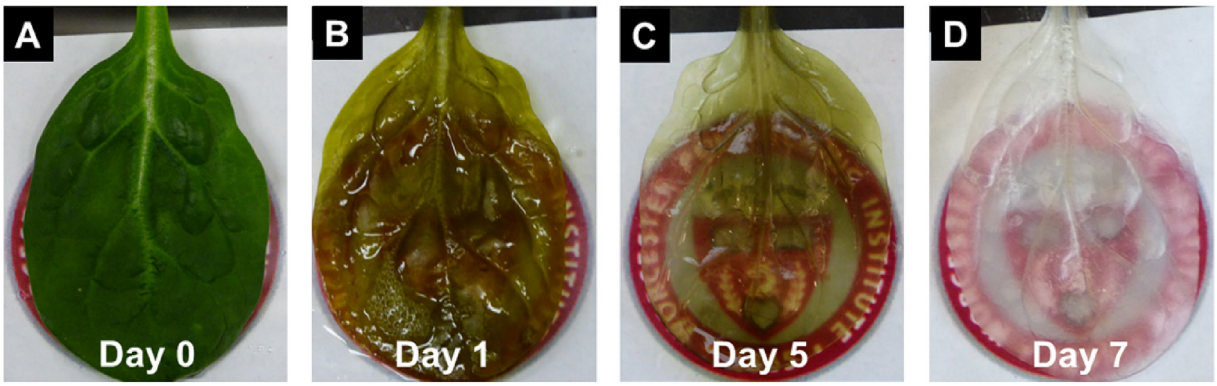

Fig. 2. Time lapse of spinach leaf decellularization. (A) Leaf is dark green and opaque prior to decellularization at Day 0. **(B)** At Day 1, the leaf loses some of its dark coloring and begins to appear translucent. **(C)** By Day 5, the leaf is completely translucent while maintaining a light green hue. **(D)** After being treated and sterilized with sodium chlorite, the leaf loses the remainder of its coloring and becomes completely decellularized on Day 7.

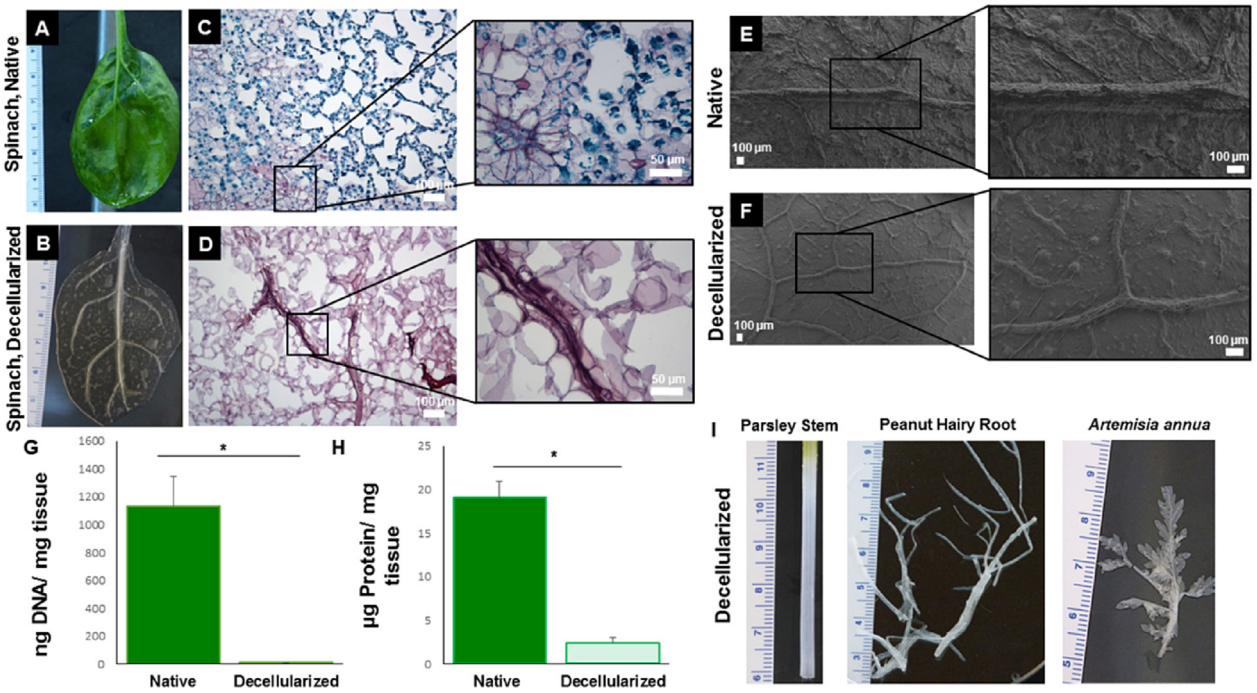

Fig. 3. Characterization of plant scaffolds before and after decellularization. Spinach leaf **(A)** before and **(B)** after decellularization; **(C)** Native and **(D)** decellularized leaf stained with Safranin and Fast Green. Safranin-O (red) stains for chromosomes and nuclei. Fast Green (bluish-green) stains for cytoplasm and cellulosic cell walls. The blue dark spheres are indicative of chloroplasts, which are highly abundant in leaves. Scale bars: 250 µm and 50 µm (insert). Scanning Electron Microscope image of surface topography for both **(E)** native and **(F)** decellularized spinach leaves with inserts showing higher magnification. Scale bars: 100 µm. **(G)** DNA content was quantified through a CyQuant assay ($p = 0.00002$; n = 4). **(H)** Total protein before and after leaf decellularization was quantified by Bradford assay ($p = 0.0000007$; n = 3). **(I)** Decellularization process was applied to other plant types and structures. (For interpretation of the references to colour in this figure legend, the reader is referred to the web version of this article.)

were acquired at 60 frames per second to visualize the microsphere flow (Fig. 4C; *To increase contrast, the bead was false-colored white in these videos*). The medium that perfused through the leaf (flow through) was collected and used to calculate the percentage of microspheres recovered by measuring fluorescence intensity. While all of the 1 and 10 µm beads were recovered after perfusion, transport of larger beads became progressively more restrictive; only 46% of the 50 µm and 10% of the 100 µm microspheres were collected (Fig. 4D). Additionally, analysis of blank fluid being perfused through the system shows some noise generated by autofluorescence, where the 100 µm microsphere collection was found to be within this noise region. Collection of the 1 and 10 µm microspheres was found to be statistically greater than both the 100 µm microsphere collection ($p = 0.01$ for 1 µm and 10 µm microspheres) and the blank fluid noise ($p = 0.009$ for 1 µm and $p = 0.01$ for 10 µm microspheres). Visualization of the entrapped beads within plant vascular networks yielded complementary results (Fig. 4E and F); i.e. only 50 and 100 µm diameter microspheres were found to be trapped within the plant tissue. Taken together, these results demonstrate that the leaf vasculature supports the flow of particles within the size range of a red blood cell.

3.3. Recellularization of decellularized leaf scaffolds with human cells

Successful use of decellularized plant tissues for human tissue

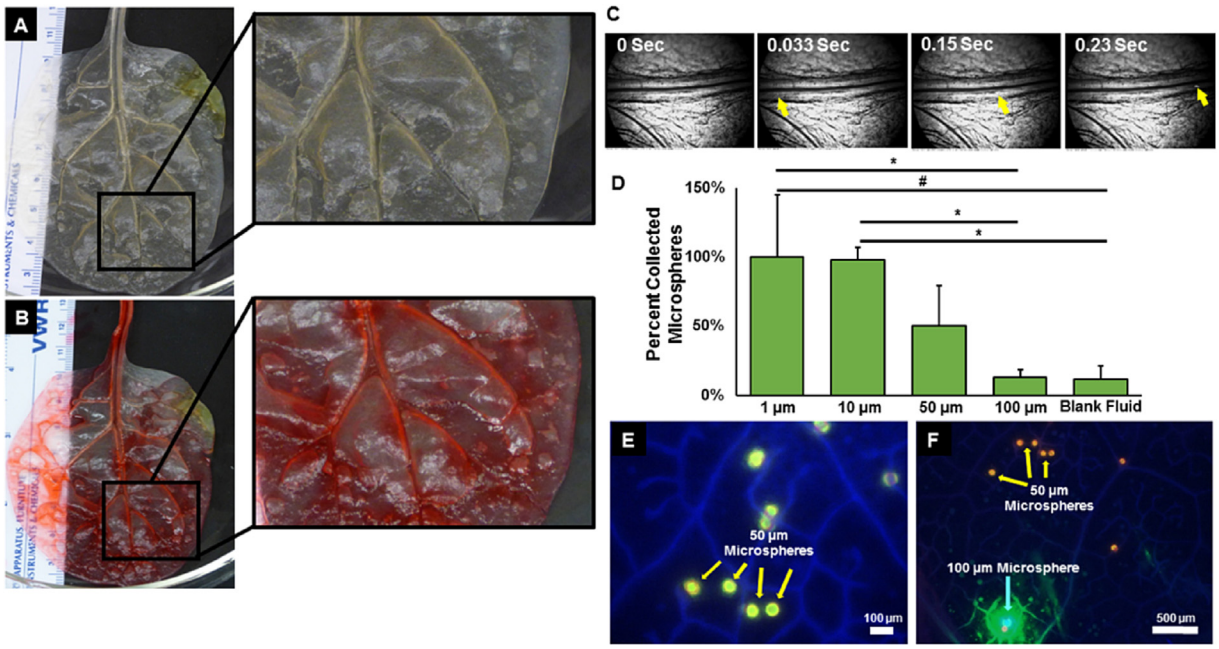

Fig. 4. Spinach leaf vascular scaffolds retain patency and perfusion capabilities after decellularization. Decellularized leaf **(A)** before and **(B)** after perfusion of Ponceau Red. Fluorescent microspheres of various diameters (1, 10, 50, and 100 μm) and blank fluid were perfused through a decellularized leaf. Statistical differences were found between the percentage collected between both 1 and 10 μm and the collection of 100 μm and blank fluid. (* indicates $p < 0.05$, # indicated $p < 0.01$). **(C)** Video frames capturing microsphere location within a leaf vein over time, with the arrow tracking an individual microsphere. **(D)** Microspheres that traversed vascular walls were collected and their fluorescence quantified (n = 3). **(E, F)** Fluorescence images of leaf vasculature perfused with beads. Images show 50 and 100 μm spheres retained within the vasculature. Scale Bars: 100 μm (E), 500 μm (F).

culture depends on the ability of human cells to adhere to plant-produced ECM. Different human cell types were seeded either on top of decellularized plant scaffolds or introduced into plant vascular networks via cannulation.

To endothelialize the leaf vasculature, human umbilical vein endothelial cells (HUVEC) were seeded into the leaf scaffold vasculature. Leaf vasculature was first coated with fibronectin in order to promote cellular attachment to the lignified walls of the leaf vasculature. HUVECs labeled with acetylated low-density lipoprotein (Dil-Ac-LDL) were delivered through the cannula. After 24 h, HUVEC attachment to the inner surface of leaf vasculature was confirmed with confocal microscopy (Fig. 5A). HUVEC viability after recellularization was evaluated using an LDL uptake assay. Unlabeled HUVECs were injected through the cannula and allowed 24 h to attach to the inner surfaces of the leaf's stem. Seeded and unseeded stems were incubated in Dil-Ac-LDL medium and fluorescent signal was assessed 24 and 48 h after incubation. At both time points, there was a positive fluorescent signal present for seeded stems and no signal for unseeded stems, indicating that the HUVECs remained viable after recellularization (Fig. S6). Although HUVECs attached and remained viable after recellularization, improvements in functionalizing the leaf vasculature and use of perfusion bioreactors will be needed before complete endothelialization of the entire leaf can occur.

Human mesenchymal stem cells (hMSC) were used for seeding onto the outside surface of a decellularized leaf (Fig. 5B). To overcome autofluorescence generated within the plant tissue, mostly seen in the shorter wavelengths of the visible spectrum [35], hMSCs were labeled with quantum dots prior to the seeding, as previously described [36]. The hMSCs readily adhered to the entire surface of the leaf 24 h after seeding. Cell attachment was also observed on the outside surface of decellularized parsley stems (Fig. S7), indicating that three-dimensional plant surfaces could be used as scaffolds, from plants with varied species or macro-scale structures. This would allow for larger and more intricate tissue to be formed on these scaffolds.

3.4. Human pluripotent stem cell-derived cardiomyocytes function on decellularized plant scaffolds

Human pluripotent stem cell derived cardiomyocytes (hPS-CM) were seeded onto the surface of leaf scaffolds in order to investigate whether cells could adhere and maintain functionality. hPS-CMs attached to the surface and formed cell clusters (Fig. 6A) within three days of seeding. Five days after the initial seeding, hPS-CMs began to spontaneously contract (Movie S3) while seeded on the leaf scaffold while control hPS-CM seeded on tissue culture plastic (TCPS) began contraction on Day 3.

Contractile analysis (Fig. 6B), based on sub-pixel level change in the random light intensity of the hPS-CM cluster [31], demonstrated approximately 1% contractile strain at a contractile rate of 0.8 Hz in the myocytes seeded on leaf scaffolds. Spatial strain maps revealed contraction present throughout the entire hPS-CM cluster whereas the surface of the scaffold displayed little to no strain signal (Fig. 6C). Contractile strain increased from Day 5 to Day 10. At Day 10, the contraction peaked and plateaued for 7 days, until Day 17. There was a decrease in contraction from Day 17 to Day 21 (Fig. 6D). On Day 21 (Fig. 6E), hPS-CM contraction decreased to 0.6% at a contractile rate of 0.5 Hz. The control hPS-CM clusters seeded onto TCPS had a higher magnitude of contractile strain on all days of analysis and these measures were found to be statistically greater on days 7 ($p = 0.04$) and 17 ($p = 0.04$). There was no statistical difference between the hPS-CM clusters on the leaf scaffolds and TCPS control for all other time points. Contractile analysis on day 10 (the peak value for the hPS-CMs seeded onto the leaf scaffold) (Fig. S8) yielded similar strain values for the cells seeded on the TCPS with contractile strains near 1.0% with a frequency of 0.37 Hz.

Due to the decrease in contraction at Day 21, we investigated

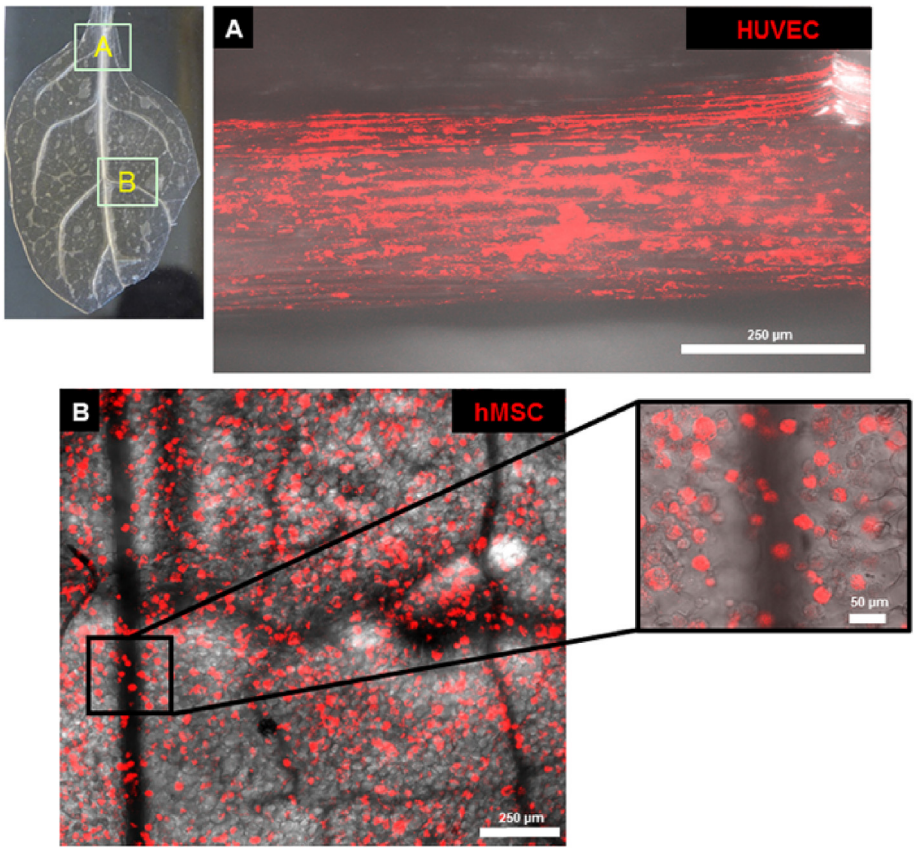

Fig. 5. Human cells can be used to recellularize the decellularized spinach leaves. The image of the leaf in the upper left corner of the image gives the relative position from which images A and B are derived. **(A)** Dil-Ac-LDL-labeled human umbilical vein endothelial cells (HUVECs) were seeded within a vein of a decellularized spinach leaf by perfusion. Scale bar: 250 μm. **(B)** Human mesenchymal stem cells (hMSCs) were labeled with quantum dots and seeded onto the surface of a decellularized spinach leaf. Scale bars: 250 μm for main image, and 50 μm for insert.

whether the calcium handling capability of these cells was maintained using GCaMP3 reported transfected hPS-CM cells [30], providing a fluorescent signal corresponding to the intracellular calcium signal. Fluorescence videos (Movie S4) detected GCaMP3 fluorescence (Fig. 6F), corresponding to calcium flux during contraction. On Day 21, the change in fluorescent signal intensity in hPS-CM clusters was measured over several contractile cycles and compared to the signal from the surface of the leaf (Fig. 6G and H). The calcium signal originating from the hPS-CM cluster was more intense than the signal from the leaf's surface, suggesting that the hPS-CMs retained calcium-handling capabilities when seeded onto the leaf scaffolds and was not an artifact of autofluorescence. Furthermore, the calcium signal also followed a similar frequency, 0.5 Hz, as seen with the contraction at Day 21 suggested that the two are interrelated and thus the cardiomyocytes are functioning normally on the leaf. The calcium signal from the hPS-CMs that were seeded on the leaf scaffolds were also compared to hPS-CMs that were seeded on TCPS at day 21 (Fig. S9). Calcium signals had similar fluorescent intensities with the hPS-CMs having a higher calcium handling frequency. This difference in frequency is probably due to the difference in the size of the different clusters analyzed as the clusters of hPS-CMs formed on the TCPS were larger than the clusters formed on the leaf scaffolds.

4. Discussion

Exploring biological “orthogonality” between kingdoms provides a unique opportunity to interface multiple biological kingdoms, as well as to mimic biological features from other kingdoms. This novel approach can be exploited in order to utilize paradigms that have evolved in one biological kingdom in order to provide solutions to problems that another kingdom faces, through a common interface. By searching for interfaces between the plant and animal systems, new solutions may be effectively engineered for a wide variety of disciplines, such as regenerative medicine.

For example, the major limiting factor affecting the clinical translation of tissue engineering is the lack of viable vascular networks in engineered tissues. Current fabrication techniques, such as 3-D printing, cannot accurately and effectively create microvasculature, such as that seen in capillary beds. With all of that in mind, we looked for inspiration from the plant kingdom to address this challenge. Plant vasculature, like mammalian vasculature, supports flow of fluid and transport of important biomolecules. This transport is accomplished through a different mechanism in the plant than in mammalian vessels, but the structures are similar, especially the microvascular architecture. Furthermore, cellulose which is the main component of plant cell walls is a well-studied polysaccharide and biomaterial. Cellulose has been used in a wide variety of regenerative medicine applications, such as cartilage tissue engineering [37,38], bone tissue engineering [39,40], and wound healing [20,21]. For those studies, cellulose was usually derived from bacteria in order to control the fiber geometries and chemical properties. More recently, however, cellulose was isolated from decellularized apple hypanthium tissue and was used to support cellular attachment and proliferation in a 3D scaffold [22]. That material was found to be biocompatible when implanted

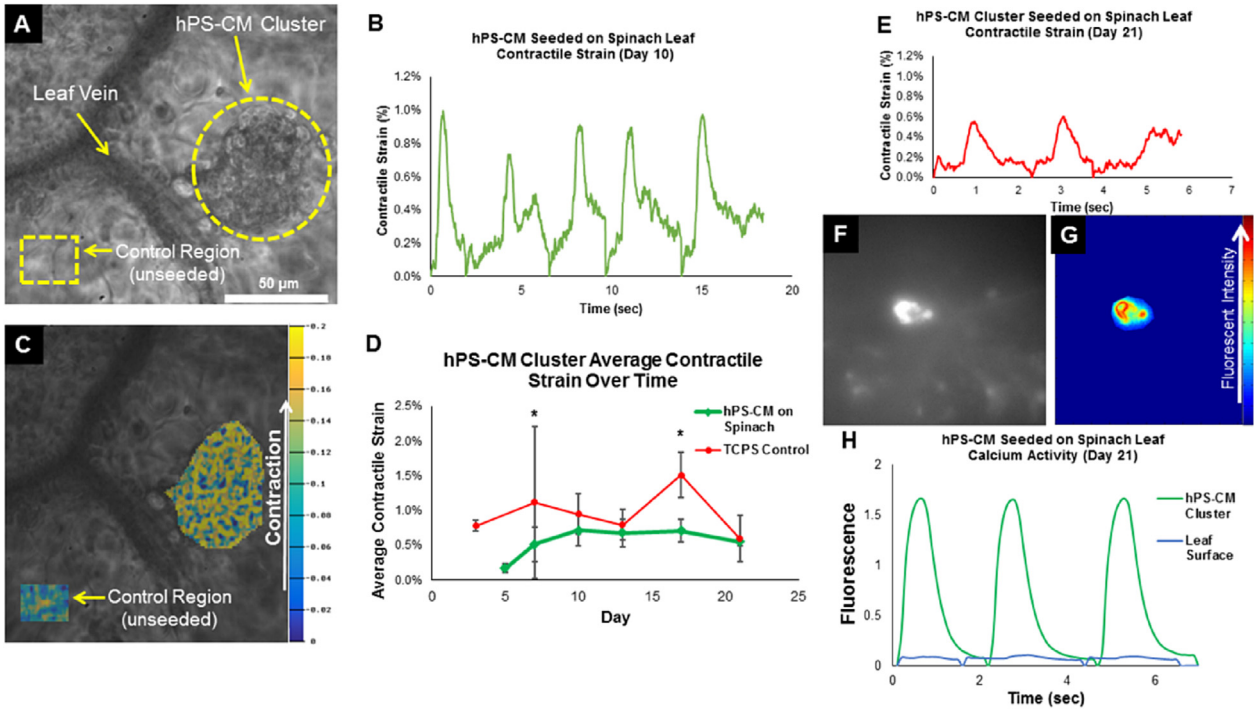

Fig. 6. Human pluripotent stem cell-derived cardiomyocytes (hPS-CMs) adhere and function on the surface of a leaf scaffold for 21 days. (A) hPS-CMs adhere and form cell clusters. Scale bar: 50 μm. **(B)** Contractile strain of hPS-CMs was quantified through subpixel level displacement of the cell clusters. Contraction was graphed over the time of recorded videos and, on Day 10, the cluster was found to contract at nearly 1% strain. **(C)** Contractile strain can be visualized through a heatmap. **(D)** Contractile strain was measured over 21 days for a cluster of cells. Contractile strain was compared to a control of hPS-CMs cultured on tissue culture plastic (TCPS). Strains calculated on days 7 and 17 were found to be statistically greater on cells seeded on the TCPS as opposed to cells seeded on the leaf scaffolds (* indicates $p < 0.05$). There were no statistical differences calculated in any of the other time points. **(E)** Day 21 strain values showing the lowered contractile strain magnitude. **(F)** hPS-CMs were modified with a GCaMP3 reporter [30], providing a fluorescent signal corresponding to the intracellular flux of calcium ions. **(G, H)** The relative change of fluorescent signal was visualized and compared relative to the leaf surface on Day 21.

subcutaneously *in vivo* [23]. Coupling the similarities seen between mammalian and plant vasculature with the apparent biocompatibility and regenerative properties of the plant tissue, we sought to *cross kingdoms* and study whether decellularized plants could serve as a perfusable scaffold for tissue engineering.

Perfusion decellularization techniques were successfully adapted for use with plant tissues. Multiple plant types, all with different hierarchical geometries, were able to be decellularized including, spinach and *A. annua* leaves, parsley stems, and peanut hairy roots. Spinach was chosen as the model leaf through the rest of the study due to its ready availability and its high vascular density. Other plant species were chosen to highlight the widespread potential of the technique. Decellularization was verified through histological staining, as well as quantification of DNA and protein content. Histological staining showed the loss of nucleic materials from the plant tissue while maintaining both the structure and the differing native composition of the tissue, as noted when lignin was stained before and after decellularization. The vasculature remained patent after decellularization, as demonstrated by microsphere perfusion. Using the microspheres, the vessel diameter of perfusable vasculature within the spinach leaves could be approximated, which was found to support flow of particles the size of human blood cells. The decellularized plant scaffolding also supported human cell recellularization. Adhered HUVECS exhibited some alignment to the inner vascular walls, and remained viable; MSCs adhered to the surface of the leaf; and hPS-CMs spontaneously contracted over the course of 21 days while attached to the surface of the leaf scaffolds.

By using the natural architecture of plant tissue, we could effectively engineer a multiplicity of mammalian tissue depending upon the plant template. Matching native mechanical properties have shown to be a crucial aspect when engineering tissue. Since a wide variety of anatomical structures exist within the plant kingdom [17], finding structures with mechanical properties emulating those needed for a human tissue engineered scaffold, even after decellularization, should be feasible. This is advantageous due to the diversity in architecture of different plants and their structures, in the hopes that they may be able to recapitulate some of the complexity seen within mammalian tissues and thus lead to future clinical applications. Further optimization and investigation would be necessary to understand which plant tissue would be appropriate for different tissue engineering applications. A highly vascularized plant tissue, such as the spinach leaf, might be better suited for a highly vascularized tissue, like cardiac tissue, whereas the cylindrical hollow structure of the stem of *Impatiens capensis* might better suit an arterial graft. Conversely, the vascular columns of wood might be useful in bone engineering due to their relative strength and geometries.

Plant based tissue engineered solutions need to be further elucidated and explored before translation into medical applications. The decellularization solutions used in this study contain high concentrations of detergents that were chosen after an initial investigation that accounted for the time needed for decellularization. Residual detergents present after decellularization have been shown to affect cellular viability [41] and thus could become problematic with use of high detergent concentrations. There were at worst only limited viability issues in this study, nevertheless, this and other potential concerns should be addressed with further refinement of the decellularization techniques.

Currently, it is as yet unclear how the plant vasculature would be integrated into the native human vasculature and whether there would be an immune response. Decellularized cellulose is

biocompatible and biodegradable [23], but it is unclear the *in vivo* response to whole decellularized plant tissue. Future investigation will need to be made into the native immune response to more complex compositional plant scaffolds. Furthermore, we have shown the ability of HUVECs to attach to the inner leaf vasculature after 24 h. To have a non-thrombogenic scaffold, full endothelialization needs must be demonstrated and there must be functionality.

The ability to fully recellularize decellularized tissue has long been a major problem in the field and future studies are needed to recellularize endothelium for plant tissue. More recent investigation into complex tissue recellularization, such as vascularization of whole lung [42], has been improving and these new techniques will be crucial in improving the medical potential of our plant scaffolds and other decellularized tissues. One final aspect of our plant scaffolds that needs to be further developed in order to improve the medical translation, is the question about out flow in the plant vasculature. Plant vasculature does not have a separate out flow system, such as the venous system. A potential tissue engineered graft based upon the plant scaffolds could use multiple leaves where some act as arterial support and some act as venous return.

The use of plants as the foundation for tissue engineering scaffolds has many benefits outside their innate vascular networks. There is a current push in technology development to become more "green" and environmentally friendly due to concerns over anthropogenic climate change and dwindling supplies of natural resources. Tissue engineered scaffolds are typically produced either from animal-derived or synthetic biomaterials, both of which have a large cost and large environmental impact. Animal-derived biomaterials used extensively as scaffold materials for tissue engineering include native ECM proteins such as collagen I or fibronectin and whole animal tissues and organs. Annually, 115 million animals [43] are estimated to be used in research. Due to this large number, a lot of energy is necessary for the upkeep and feeding of such animals as well as to dispose of the large amount of waste that is generated. Along with this environmental impact, animal research also has a plethora of ethical considerations, which could be alleviated by forgoing animal models in favor of more biologically relevant *in vitro* human tissue models.

Synthetic biomaterials are commonly generated from chemical processing of nonrenewable resources, such as petroleum, and their production often yields toxic byproducts. An example of a biomaterial negatively affecting the environment can be found from polytetrafluoroethylene (Teflon), a widely used synthetic biomaterial in cardiovascular applications such as tissue engineered vascular grafts [44]. During high temperature degradation of Teflon, large amounts of ozone-depleting gases such as trifluroacetic acid and chlorodifluoroacetate [45] are generated. While this is not an issue in the body when Teflon is used as a graft, manufacturing byproducts are a major concern for the production and storage of the material. Recently, more eco-friendly sources for biomaterial production have been explored, such as syntheses from vegetable oils [46] and polymerization of natural bio-polymers like cellulose [47]. By exploiting the benign chemistry of plant tissue scaffolds, we could address the many limitations and high costs of synthetic, complex composite materials. Furthermore, there are many issues in the mass production of materials that could be overcome from using plant tissue. Plants can be easily grown using good agricultural practices (GAP) and under controlled environments. By combining environmentally friendly plant tissue with perfusion-based decellularization, we have shown that there can be a sustainable solution for pre-vascularized tissue engineering scaffolds.

In this study, we demonstrated the feasibility of using decellularized plants to provide sustainably produced scaffolding for tissue engineering. By applying paradigms from one kingdom to another, we devised a method for addressing the limitation of perfusion that exists in traditional approaches to tissue engineering and regenerative medicine. Our investigation provided promising results, but many questions still remain before decellularized plants become clinically relevant. The development of decellularized plants for scaffolding opens up the potential for a new branch of science that investigates the mimicry between kingdoms, e.g. between plant and animal. Although further investigation is needed to understand future applications of this new technology, we believe it has the potential to develop into a "green" solution pertinent to a myriad of regenerative medicine applications.

Author contributions

J.R.G. performed and analyzed decellularization protocols, perfusion studies, mammalian recellularization, hPS-CM contraction analysis, and mechanical testing. S.H., S.A.L., and D.M.D. acquired and analyzed DNA and protein content. G.F. acquired SEM images. L.R.P. performed and analyzed histological staining. K.J.H. acquired and analyzed hPS-CM contraction. B.Y.K.B. acquired PEG/fluorescein images. T.Y. and F.M – B cultured and decellularized peanut hairy roots. P.J.W. and C.L.C. provided plant biology supervision. M.W.R. provided advice on experimental design and data analysis. T.D. and W.L.M. provided tissue engineering supervision. J.R.G. and G.R.G. designed the study. J.R.G. collected and assembled the data. G.R.G. supervised the study. J.R.G., P.J.W., T.D., G.R.G. wrote the manuscript. All authors reviewed and commented on the manuscript.

Acknowledgments

The authors would like to thank Dr. Michael Laflamme (University of Toronto) for kindly providing the hPS-CMs used in this study. This work is supported in part by the National Heart, Lung, and Blood Institute (R01HL115282 to G.R.G.) and National Science Foundation (DGE1144804 to J.R.G., S.H., K.J.H., D.M.D., M.W.R., T.D., G.R.G.). The authors declare that they have no competing interests. All the data needed to evaluate the conclusions made in this paper are present within the data presented in the paper and/or the Supplemental Materials. Additional data may be requested from the authors.

Appendix A. Supplementary data

Supplementary data related to this article can be found at http://dx.doi.org/10.1016/j.biomaterials.2017.02.011.

References

[1] Introduction, Am. J. Transplant. 16 (2016) 8–10, http://dx.doi.org/10.1111/ajt.13665.
[2] R.K. Jain, P. Au, J. Tam, D.G. Duda, D. Fukumura, Engineering vascularized tissue, Nat. Biotechnol. 23 (2005) 821–823, http://dx.doi.org/10.1038/nbt0705-821.
[3] M.C. Peters, P.J. Polverini, D.J. Mooney, Engineering vascular networks in porous polymer matrices, J. Biomed. Mater. Res. 60 (2002) 668–678.
[4] H. Gerhardt, VEGF and endothelial guidance in angiogenic sprouting, Organogenesis 4 (2008) 241–246.
[5] J.T. Borenstein, H. Terai, K.R. King, E.J. Weinberg, M.R. Kaazempur-Mofrad, J.P. Vacanti, Microfabrication technology for vascularized tissue engineering, Biomed. Microdevices 4 (2002) 167–175, http://dx.doi.org/10.1023/A:1016040212127.
[6] H.C. Ott, T.S. Matthiesen, S.-K. Goh, L.D. Black, S.M. Kren, T.I. Netoff, et al., Perfusion-decellularized matrix: using nature's platform to engineer a bioartificial heart, Nat. Med. 14 (2008) 213–221, http://dx.doi.org/10.1038/nm1684.
[7] J.R. Gershlak, J.I.N. Resnikoff, K.E. Sullivan, C. Williams, R.M. Wang, L.D. Black, Mesenchymal stem cells ability to generate traction stress in response to

substrate stiffness is modulated by the changing extracellular matrix composition of the heart during development, Biochem. Biophys. Res. Commun. 439 (2013) 161–166, http://dx.doi.org/10.1016/j.bbrc.2013.08.074.
[8] J.P. Guyette, J. Charest, R.W. Mills, B. Jank, P.T. Moser, S.E. Gilpin, et al., Bioengineering human myocardium on native extracellular matrix, Circulation Res. 118 (2015) 56–72, http://dx.doi.org/10.1161/CIRCRESAHA.115.306874. CIRCRESAHA.115.306874.
[9] J.J. Song, H.C. Ott, Organ engineering based on decellularized matrix scaffolds, Trends Mol. Med. 17 (2011) 424–432.
[10] K.E. Sullivan, K.P. Quinn, K.M. Tang, I. Georgakoudi, L.D. Black III, Extracellular matrix remodeling following myocardial infarction influences the therapeutic potential of mesenchymal stem cells, Stem Cell Res. Ther. 5 (2014) 1–16, http://dx.doi.org/10.1186/scrt403.
[11] T.W. Gilbert, T.L. Sellaro, S.F. Badylak, Decellularization of tissues and organs, Biomaterials 27 (2006) 3675–3683, http://dx.doi.org/10.1016/j.biomaterials.2006.02.014.
[12] T.D. Johnson, R.C. Hill, M. Dzieciatkowska, V. Nigam, A. Behfar, K.L. Christman, et al., Quantification of decellularized human myocardial matrix: a comparison of six patients, Proteomics Clin. Appl. 10 (2016) 75–83, http://dx.doi.org/10.1002/prca.201500048.
[13] S.E. Gilpin, J.P. Guyette, G. Gonzalez, X. Ren, J.M. Asara, D.J. Mathisen, et al., Perfusion decellularization of human and porcine lungs: bringing the matrix to clinical scale, J. Heart Lung Transpl. 33 (2014) 298–308, http://dx.doi.org/10.1016/j.healun.2013.10.030.
[14] S.F. Badylak, D. Taylor, K. Uygun, Whole-organ tissue engineering: decellularization and recellularization of three-dimensional matrix scaffolds, Annu. Rev. Biomed. Eng. 13 (2011) 27–53, http://dx.doi.org/10.1146/annurev-bioeng-071910-124743.
[15] K.A. McCulloh, J.S. Sperry, F.R. Adler, Water transport in plants obeys Murray's law, Nature 421 (2003) 939–942, http://dx.doi.org/10.1038/nature01444.
[16] C.D. Murray, The physiological principle of minimum work: I. the vascular system and the cost of blood volume, Proc. Natl. Acad. Sci. U.S.A. 12 (1926) 207–214.
[17] L.J. Gibson, The hierarchical structure and mechanics of plant materials, J. R. Soc. Interface 9 (2012), http://dx.doi.org/10.1098/rsif.2012.0341 rsif20120341–2766.
[18] I. Levental, P.C. Georges, P.A. Janmey, Soft biological materials and their impact on cell function, Soft Matter 3 (2007) 299–306.
[19] F.A. Pettolino, C. Walsh, G.B. Fincher, A. Bacic, Determining the polysaccharide composition of plant cell walls, Nat. Protoc. 7 (2012) 1590–1607, http://dx.doi.org/10.1038/nprot.2012.081.
[20] W.K. Czaja, D.J. Young, M. Kawecki, R.M. Brown, The future prospects of microbial cellulose in biomedical applications, Biomacromolecules 8 (2007) 1–12, http://dx.doi.org/10.1021/bm060620d.
[21] W. Czaja, A. Krystynowicz, S. Bielecki, R.M. Brown, Microbial cellulose—the natural power to heal wounds, Biomaterials 27 (2006) 145–151, http://dx.doi.org/10.1016/j.biomaterials.2005.07.035.
[22] D.J. Modulevsky, C. Lefebvre, K. Haase, Z. Al-Rekabi, A.E. Pelling, Apple derived cellulose scaffolds for 3D mammalian cell culture, PLoS ONE 9 (2014) e97835, http://dx.doi.org/10.1371/journal.pone.0097835.
[23] D.J. Modulevsky, C.M. Cuerrier, A.E. Pelling, Biocompatibility of subcutaneously implanted plant-derived cellulose biomaterials, PLoS ONE 11 (2016) e0157894, http://dx.doi.org/10.1371/journal.pone.0157894.
[24] F. Munarin, S.G. Guerreiro, M.A. Grellier, M.C. Tanzi, M.A. Barbosa, P. Petrini, et al., Pectin-based injectable biomaterials for bone tissue engineering, Biomacromolecules 12 (2011) 568–577, http://dx.doi.org/10.1021/bm101110x.
[25] L.M. Ferreira, C.S. Sobral, L. Blanes, M.Z. Ipolito, E.K. Horibe, Proliferation of fibroblasts cultured on a hemi-cellulose dressing, J. Plast. Reconstr. Aesthet. Surg. 63 (2010) 865–869, http://dx.doi.org/10.1016/j.bjps.2009.01.086.
[26] J. Condori, G. Sivakumar, J. Hubstenberger, M.C. Dolan, V.S. Sobolev, F. Medina-Bolivar, Induced biosynthesis of resveratrol and the prenylated stilbenoids arachidin-1 and arachidin-3 in hairy root cultures of peanut: effects of culture medium and growth stage, Plant Physiol. Biochem. 48 (2010) 310–318, http://dx.doi.org/10.1016/j.plaphy.2010.01.008.
[27] T. Yang, L. Fang, C. Nopo-Olazabal, J. Condori, L. Nopo-Olazabal, C. Balmaceda, et al., Enhanced production of resveratrol, piceatannol, Arachidin-1, and Arachidin-3 in hairy root cultures of peanut Co-treated with methyl jasmonate and cyclodextrin, J. Agric. Food Chem. 63 (2015) 3942–3950, http://dx.doi.org/10.1021/jf5050266.
[28] S.E. Ruzin, Plant Microtechnique and Microscopy, Oxford University Press, 1999.
[29] C. Hawes, P.B. Gahan, Plant Histochemistry and Cytochemistry: an Introduction, 1985.
[30] J.J.H. Chong, X. Yang, C.W. Don, E. Minami, Y.-W. Liu, J.J. Weyers, et al., Human embryonic-stem-cell-derived cardiomyocytes regenerate non-human primate hearts, Nature 510 (2014) 273–277, http://dx.doi.org/10.1038/nature13233.
[31] D.J. Kelly, E.U. Azeloglu, P.V. Kochupura, G.S. Sharma, G.R. Gaudette, Accuracy and reproducibility of a subpixel extended phase correlation method to determine micron level displacements in the heart, Med. Eng. Phys. 29 (2007) 154–162, http://dx.doi.org/10.1016/j.medengphy.2006.01.001.
[32] P.M. Crapo, T.W. Gilbert, S.F. Badylak, An overview of tissue and whole organ decellularization processes, Biomaterials 32 (2011) 3233–3243, http://dx.doi.org/10.1016/j.biomaterials.2011.01.057.
[33] M.P. Wiedeman, Dimensions of blood vessels from distributing artery to collecting vein, Circulation Res. 12 (1963) 375–378, http://dx.doi.org/10.1161/01.RES.12.4.375.
[34] Y.C. Fung, B.W. Zweifach, Microcirculation: mechanics of blood flow in capillaries, Annu. Rev. Fluid Mech. 3 (1971) 189–210.
[35] M.D. Fricker, N.S. White, Wavelength considerations in confocal microscopy of botanical specimens, J. Microsc. 166 (1992) 29–42, http://dx.doi.org/10.1111/j.1365-2818.1992.tb01505.x.
[36] J.P. Guyette, M. Fakharzadeh, E.J. Burford, Z.-W. Tao, G.D. Pins, M.W. Rolle, et al., A novel suture-based method for efficient transplantation of stem cells, J. Biomed. Mater Res. A 101 (2013) 809–818, http://dx.doi.org/10.1002/jbm.a.34386.
[37] A. Svensson, E. Nicklasson, T. Harrah, B. Panilaitis, D.L. Kaplan, M. Brittberg, et al., Bacterial cellulose as a potential scaffold for tissue engineering of cartilage, Biomaterials 26 (2005) 419–431, http://dx.doi.org/10.1016/j.biomaterials.2004.02.049.
[38] F.A. Müller, L. Müller, I. Hofmann, P. Greil, M.M. Wenzel, R. Staudenmaier, Cellulose-based scaffold materials for cartilage tissue engineering, Biomaterials 27 (2006) 3955–3963, http://dx.doi.org/10.1016/j.biomaterials.2006.02.031.
[39] J. Liuyun, L. Yubao, Preparation and biological properties of a novel composite scaffold of nano-hydroxyapatite/chitosan/carboxymethyl cellulose for bone tissue engineering, J. … 16 (2009).
[40] M. Zaborowska, A. Bodin, H. Bäckdahl, J. Popp, A. Goldstein, P. Gatenholm, Microporous bacterial cellulose as a potential scaffold for bone regeneration, Acta Biomater. 6 (2010) 2540–2547, http://dx.doi.org/10.1016/j.actbio.2010.01.004.
[41] B. Zvarova, F.E. Uhl, J.J. Uriarte, Z.D. Borg, A.L. Coffey, N.R. Bonenfant, et al., Residual detergent detection method for nondestructive cytocompatibility evaluation of decellularized whole lung scaffolds, Tissue Eng. Part C Methods 22 (2016) 418–428, http://dx.doi.org/10.1089/ten.TEC.2015.0439.
[42] X. Ren, P.T. Moser, S.E. Gilpin, T. Okamoto, T. Wu, L.F. Tapias, et al., Engineering pulmonary vasculature in decellularized rat and human lungs, Nat. Biotechnol. 33 (2015) 1097–1102, http://dx.doi.org/10.1038/nbt.3354.
[43] K. Taylor, N. Gordon, G. Langley, W. Higgins, Estimates for worldwide laboratory animal use in 2005, Atla 36 (2008) 327.
[44] H. Shin, S. Jo, A.G. Mikos, Biomimetic materials for tissue engineering, Biomaterials 24 (2003) 4353–4364.
[45] D.A. Ellis, S.A. Mabury, J.W. Martin, D.C. Muir, Thermolysis of fluoropolymers as a potential source of halogenated organic acids in the environment, Nature 412 (2001) 321–324, http://dx.doi.org/10.1038/35085548.
[46] S. Miao, P. Wang, Z. Su, S. Zhang, Vegetable-oil-based polymers as future polymeric biomaterials, Acta Biomater. 10 (2014) 1692–1704, http://dx.doi.org/10.1016/j.actbio.2013.08.040.
[47] A. Gandini, Polymers from renewable resources: a challenge for the future of macromolecular materials, Macromolecules 41 (2008) 9491–9504, http://dx.doi.org/10.1021/ma801735u.